Characterization of Sulphated Cellulose Nanocrystals as Stabilizer for Magnetite Nanoparticles Synthesis with improved Magnetic Properties

[1]**Omorogbe** Stanley O.,***Ikhuoria** Esther U., **Igiehon** Lauretta I., **Agbonlahor** Osazuwa G., [1]**Ifijen** Hilary I., [1]**Aigbodion** Aireguamen I.

Department of Materials Chemistry, University of Benin, Benin-City. 300213, Nigeria.
[1]Rubber Research Institute of Nigeria. Benin City. 300272, Nigeria

[*]Corresponding author: esyikhuoria@yahoo.com.

Abstract

This work reports on hydrogen bond energy of sulphated cellulose nanocrystals (CNC) obtained from rubber wood (RW) cellulose for effective steric stabilization of magnetite nanoparticles obtained *via* the modified Massart's method. The particles morphology, structure and crystallite properties were investigated by using microscopic techniques. The magnetic properties of Fe_3O_4 nanoparticles were investigated by using physical property measurement system. The average width of CNC was ≈20 nm with length of between 190 nm-300 nm. Changes in the hydrogen bond energy of the RW cellulose, during acid hydrolysis, were investigated by using the FT-IR hydrogen bonding energy calculation. The CNCs capped Fe_3O_4 particles synthesized, were monodispersed and oval in shape (with average particle diameter of ≈4 nm). The Fe_3O_4nanoparticles obtained, exhibited superparamagnetic behaviour and saturation magnetization (*M*s) of ≈67.5 amu/g.

Keywords: Sulphated cellulose nanocrystals, Stabilizer, Magnetite nanoparticles, Magnetic properties, Monodispersibilty, Rubber wood (RW), Biocompatibility

1. INTRODUCTION

Nanocellulose exhibits unique properties, such as: crystallinity, strength, bio-compatibility and the presence of readily functionalized surface hydroxyl groups. These properties have made it one of the most researched biopolymers in recent times (Moon *et al*., 2011) and necessitated various research efforts for the application of nanocellulose in advanced materials fabrication (Moon *et al*., 2011; Habibi *et al.*, 2010). Notable applications of nanocellulose, include its use as a composite material with: polysiloxanes (Grunert and Winter, 2002), polysulphonates (Oksman and Sain, 2006), polycapro-lactone (Habibi *et al.*, 2008), carboxymethyl cellulose (Choi and Simonsen, 2006), among others. (Cao *et al.,* 2007; Garcia de Rodriguez *et al.,* 2006; Habibi *et al.,* 2010; Hubbe *et al., 2008;* Paralikar *et al.,* 2008*).*

Generally, the suitability of the nanocellulose obtained, to the various intended applications and its dispersibility in the proposed matrix, is dependent, to a large extent, on its surface properties, which could vary with the synthetic method applied (Habibi *et al.*, 2010). The general synthetic routes, usually employed in the synthesis of nanocellulose are either mechanical or chemical (Zhan *et al.,* 2012). Nanocellulose crystals obtained *via* acid hydrolysis are also known to exhibit improved surface properties that are dependent on the nature of the acid used; with sulphuric acid producing particles more readily dispersed in aqueous medium when compared to hydrochloric acid-hydrolysed particles, which readily flocculate. (Habibi *et al.,* 2010; Moon *et al*., 2011). This was attributed to the fact that sulphonation of the pendant hydroxyl groups on the nanocellulose surface, results in improved particle-particle repulsion due to a strengthening of the electric double layer around the nanocellulosic crystals (Habibi *et al.*, 2010). The ability of the pendant hydroxyl group of nanocellulose to be readily functionalized, provides a means of tailoring the hydrogen bonding interaction in cellulose, thereby making it suitable for applications in steric stabilization (Habibi *et al.*, 2010).

This ability of nanocellulose to act as a steric stabilizer can promote monodispersibilty, especially magnetic materials, which can be prone to particle aggregation (Wang *et al.,* 2010; Ikhuoria *et al.,* 2015). Several synthetic methods have been employed to overcome the problem of aggregation and oxidation in magnetic nanoparticles, especially magnetite nanoparticles (Mosayebi *et al.,* 2017). High temperature synthesis remains widely reported and it involves the application of organic precursors, surfactants or a combination of these (Ravikumar and Bandyopa-dhyaya, 2011). Chemical co-precipitation remains the simplest, convenient and a cost-effective approach, if carefully monitored.

The ability of the co-precipitation process to occur in aqueous medium has made it of particular interest in the production of nanomagnetite suitable for drug delivery applications Ravikumar and Bandyopa-dhyaya, 2011; Laurent *et al.,* 2008). Notable research efforts at overcoming aggregation of nanomagnetite particles in aqueous medium, include the use of steric stabilizers,

such as: dextran, polyacrylic acid, polyvinylalcohol, citric acid, silica , gluconic acid, dimer-captosuccinic acid, among others (Laurent *et al.,* 2008; Ravikumar and Bandyopa-dhyaya, 2011; Mahmoudi *et al.,* 2008; Lin *et al.,* 2005). These stabilizers are known to prevent or reduce aggregation by using their functional groups to interact with magnetite *via* the surface hydroxyl groups of magnetite that are present in aqueous magnetite ferrofluids (Mosayebi *et al.,* 2017). Therefore, with the aid of this interaction, stabilizers can interact with magnetite to form core-shell particles (i.e. magnetite core and stabilizer shell particles), hence facilitating the dispersion of magnetite (Mosayebi *et al.,* 2017; Mondini *et al.,* 2008; Shukla *et al.,* 2007). Previous research efforts at controlling aggregation had varying degree of success, however, the use of high amounts of toxic surfactants and the cost of some of the stabilizers remains a challenge (Laurent *et al.,* 2008; Ravikumar and Bandyopa-dhyaya, 2011). Furthermore, the chemical co-precipitation route also has the general drawback of producing polydispersed particles with relatively large particle size regime (Mosayebi *et al.,* 2017; Ravikumar and Bandyopa-dhyaya, 2011). Considering the non-toxic nature of nanocellulose, coupled with its low cost, functionalized surface, bio-compatibility and crystallinity, it can present a means of overcoming particle aggregation and hence, controlling the polydispersity of nanomagnetite obtained *via* the co-precipitation method, through adequate tuning of the cellulose degree of hydrogen bonding.

This work studies the hydrogen bonding energy interaction of cellulose, tuned *via* sulphuric acid hydrolysis of rubber wood (RW) cellulose to, effectively stabilize magnetite nanoparticles. Furthermore, the crystal structure and surface morphology of CNC, CNC-capped Fe_3O_4 particles were investigated by using electron diffraction and imaging techniques. The ability of sulphated CNC to promote a relatively smaller size, and improved monodispersity of the CNC capped nanomagnetite when compared to some previous reports that employed some other surfactants, was clearly shown.

EXPERIMENTAL

Materials and Sample Preparation

Toluene, acetone, ethanol, NaOH (97%) were obtained from Sigma Aldrich Inc. USA and deionized water, sodium chlorite, glacial acetic acid, sulphuric acid, $FeCl_2$, $FeCl_3$ and Type 1, ultrapure de-ionized water (18.2 MΩ.cm, 25°C), Merck Millipore, Germany) were used. All reagents were used without further purification. Rubber wood was obtained from the Rubber Research Institute of Nigeria (RRIN), Iyanomo, Edo State. Nigeria.

Preparation of Cellulose

Extraction of waxes, oils and resins

About 50 g of RW was placed in a 500 mL Soxhlet apparatus and was extracted over a mixture of toluene, acetone and ethanol in a ratio of 4:1:1, for 7hrs in order to remove waxes, oil and resin. The RW was thereafter, washed with warm water (45-50°C) to remove other forms of impurities and dried under a vacuum oven prior to further characterization and fractionation of cellulose.

Delignification of RW

RW pulp was placed in 1.5 wt/vol % of sodium chlorite ($NaClO_2$) with drop-wise addition of acetic acid (pH < 4). The solution became bright yellow with the samples floating. The reaction was kept at a temperature of 90°C for over 4 hrs. This process was repeated two more times, until the solution became yellow and the pH remained constant. The solution was washed several times by using a Buckner funnel until a neutral pH was reached. Holocellulose (α-cellulose and β-hemicellulose) was obtained, by the gradual removal of lignin (Habibi *et al.*, 2010; Ikhuoria *et al.,* 2015).

Degrading of Hemi-Cellulose

The holocellulose obtained from delignification of RW was treated with 17 % NaOH solution. The sample was stirred for 45-60 min. The cellulose obtained was washed with de-ionized water and the conductivity was checked repeatedly in order to ensure complete removal of NaOH. The wet cellulose obtained was stored at 4°C.

Cellulose Nano-Crystals (CNC) Preparation via Acid Hydrolysis

CNC was prepared according to a previously reported procedure (Favier *et al.,* 1995; Sebe *et al.,* 2012). In a typical experiment, 3 g of cellulose was hydrolysed by 64% sulphuric acid. This hydrolysis was achieved by adding concentrated sulphuric acid drop-wise to RW cellulose suspension in an ice bath in order to reach the desired concentration with vigorous stirring for 20 min. The suspension was heated to 45°C for 70 min. The resulting suspension with excess sulphuric acid was centrifuged (by using a Remy cooling centrifuge 12°C) repeatedly (for 10 min, at 12000 rpm) until the supernatant became turbid after repeated cycles. The turbid suspension was placed in a 11 kDa MWCO dialysis membrane and dialyzed against ultrapure deionized water until a constant pH was attained after three days. The suspension was sonicated for 15 min. The resulting CNC was divided into two parts, one for freeze drying and other was diluted to a concentration of 0.5% w/w with deionised water for further characterization.

Preparation of magnetite nanoparticles by chemical coprecipitation

Magnetite was prepared by using the modified Massart's method (Durdureanu-Angheluta *et al.,* 2012; Massart *et al,* 1995). In the synthesis process, 0.01mol $FeCl_2.4H_2O$ and 0.02 mol $FeCl_3$ solutions were prepared in ultrapure deionized water in a round bottom flask and heated at

60°C for 10 min with continuous N_2 purging in order to prevent oxidation. Subsequently, 2M NaOH was added drop-wise into the ferrite solution under vigorous stirring (1200 rpm) until the pH of solution was about 12. Thereafter, 5 ml of 0.5% w/w nanocellulose was gradually added to the ferrite solution for the steric stabilization of the Fe_3O_4 nanoparticles. The mixture was subsequently heated at a temperature of 80°C for another 2 hrs. The resulting Fe_3O_4 nanoparticles formed (black precipitate) were separated magnetically after repeated washing with deionized water until a neutral pH was attained. It was then dried under vacuum at 60°C for 6 hrs.

Characterization Methods

Fourier Transform-Infrared Studies for CNC

Perkin-Elmer Spectrum One FT-IR spectrometer, operating between 4500 and 400 cm^{-1} was used to determine the functional groups present in the CNC. A resolution of 4 cm^{-1} was used and 64 scans were performed for each spectrum. The IR spectra were recorded as KBr pellets by subtracting the spectral of the KBr from the iron oxide nanoparticles.

X-ray Diffraction Studies for Magnetite

Powder X-ray diffraction studies were performed in order to determine the crystal structure of the CNC and CNC-capped synthesized magnetite nanoparticles. The diffraction pattern was recorded in a 2θ angle range of between 25-70° at a scanning range of 0.02% on an X-ray diffractometer (Philip's X'pertPro) with a CuK_α radiation (λ = 0.154) by employing an X'celerator detector and a monochromator at the diffraction beam side. Powder samples were used by employing a standard sample holder.

Crystallinity Index (CI) Studies for CNC

The crystallinity index (CI) was calculated by using the intensity values of the diffraction peaks, corresponding to the crystalline and amorphous regions, according to the Segal method (Abraham *et al.,* 2013):

$$CI = (I_{(002)} - I_{(am)}) / I_{(002)} \times 100 \quad \text{.....(1)}$$

where $I_{(002)}$ is the counter reading at peak intensity of 2θ angle close to 22.6°, representing the crystalline material and $I_{(am)}$ is the counter reading at peak intensity of 2θ angle close to 18°, representing amorphous material in natural rubber wood cellulosic fibre.

The crystallinity index was also evaluated by the method proposed by Hermans *et al.* (Rosa *et al.,* 2010)),

$$CI' = A_{cryst} / A_{tot} \quad \text{.....(2)}$$

where A_{cryst} denotes the sum area of the crystalline peaks at (101), (10$\bar{1}$), (021) and (002) crystallographic planes and $A_{tot.}$ denotes the sum area covered by the diffractogram.

Transmission Electron Microscopy (TEM) Analysis

Transmission electron microscopy (TEM) was performed in an FEI TECNAIS Twin microscopy with an accelerating voltage of 100 kV. The sample solutions were prepared by dispersion under an ultrasonic vibrator. The sample was drop casted on a 400-mesh copper grid and dried under vacuum at room temperature.

3. RESULTS AND DISCUSSION

The Fourier transform infrared (FT-IR) spectra of the rubber wood (RW), cellulose (Cell) and the CNC samples are shown in Figure 1. Infra-red spectra of lignocellulosic materials are generally categorized into two regions *viz*: the region characteristic of O-H and C-H stretching vibrations (3600-2700 cm^{-1}) and the 'finger print' region (1800-600 cm^{-1}) for cellulosic materials. The RW, Cell and CNC samples showed absorption bands corresponding to O-H vibrations at frequencies of 3426 cm^{-1}, 3420 cm^{-1}, and 3418 cm^{-1}, respectively. The peaks between 2941cm^{-1}-2944 cm^{-1} (Figure 1), are characteristics of the C-H stretching vibrations in methyl and methylene groups of cellulosic materials (Ikhuoria *et al,* 2015; Favier *et al.,* 1995; Abraham *et al.,* 2013; Rosa *et al*., 2010). The band at 1737 cm^{-1} (in the RW spectra) is typical of C=O stretching vibrations of hemicellulose carboxyl and acetyl groups. The absence of this band in the cellulose and CNC spectra confirms the removal of hemicellulose during the fractionation process of RW. The bands at 1596 cm^{-1}, 1508 cm^{-1} and 1235 cm^{-1} (in RW spectra) are typical of the C=C stretching vibrations of benzene and guaiacyl/syringyl groups of lignin.

The absence of these bands also in the CNC and cellulose spectra confirms the removal of lignin during the delignification process. The peaks at about 1050-1056 cm^{-1} and between 1429-1430 cm^{-1}, are typically

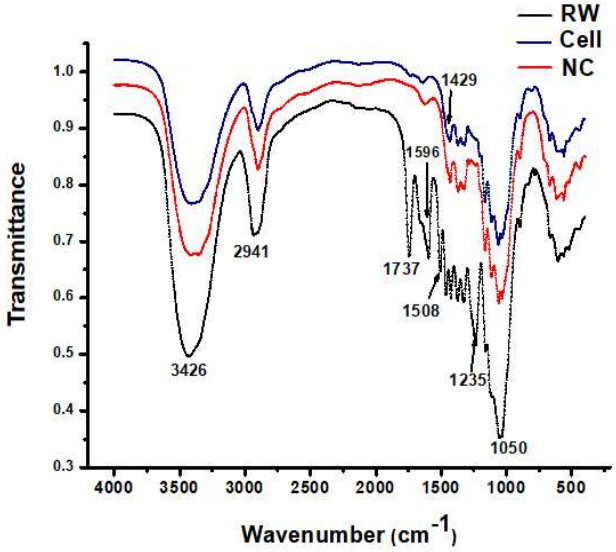

Figure 1: The FT-IR spectra of: rubber wood (RW), cellulose (Cell) and nanocellulose (CNC)

attributed to C-H, C-O deformation, stretching and bending vibrations in various carbohydrate functional groups.

Characteristic lignocellulosic peaks corresponding to C-H deformations and C-O-C stretching vibrations were observed in all three spectra at about 896-897 cm^{-1} and 1160-1162 cm^{-1}, respectively. The peaks between 1614-1616 cm^{-1} and between 668-670 cm^{-1}, correspond to OH bending (of absorbed water) and C-OH out-of-plane bending (of cellulose) (Chen *et al.,* 2009; Poletto *et al.,* 2014; Popescu *et al.,* 2007).

An index for comparing the degree of hydrogen bonding is the energy of the hydrogen bond, which monitors the deviation of the O-H absorption band from that expected for the free O-H stretching vibration. A comparison of the O-H absorption band of the RW, cellulose and CNC, showed that CNC had a slightly lower absorption frequency. This may be attributed to the slightly higher degree of hydrogen bonding in CNC when compared to RW and Cellulose as seen in their hydrogen bond energies (Table 1).The energy of the hydrogen bonds can be calculated (Chen *et al.,* 2009; Poletto *et al.,* 2014; Popescu *et al.,* 2007) by using Equation (3):

$$EH = 1/K[(\nu_o - \nu)/\nu_o] \quad \text{.....(3)}$$

where v_o is the frequency assigned to free hydroxyl groups (3650 cm^{-1}), v is the observed frequency for the hydrogen bonded hydroxyl groups and k denotes a constant ($1/k = 2.625 \times 10^2$ kJ).

The hydrogen bond distance (R), was estimated by using the Pimentel and Sederholm equation (Equation 4 below) (Ikhuoria *et al,* 2015; Poletto *et al.,* 2012):

$$\Delta\nu(cm^{-1}) = 4430 \times (2.84 - R) \quad \text{.....(4)}$$

where $\Delta\nu(cm^{-1}) = (\nu_o - \nu)$, ν_o is the monomeric OH stretching frequency with a value of 3600 cm^{-1} and v is the observed frequency in the IR spectra.

Table 1: Parameters from FT-IR analysis of: rubber wood (RW), cellulose (Cell) and nanocellulose (CNC)

FT-IR Indices	E_H (kJ)	R(Å)	IR Crystallinity Ratio		HBI A3435/A1317
			LOI H1430/H894		
			TCI H1367/H2914		
RW	16.11	2.800	1.6168	1.5129	1.3521
Cellulose	16.54	2.790	1.2813	1.2500	1.7273
CNC	16.69	2.796	1.5417	1.3160	1.9612

Table 1 shows the IR parameters evaluated from the FT-IR spectra. The hydrogen bond energy (E_H) and hydrogen bond distance (R), obtained for RW, Cellulose and CNC, were (16.11 kJ, 2.800 Å), (16.54 kJ, 2.790 Å), (16.69 kJ, 2.796 Å), respectively. The E_H for CNC was slightly higher than that for cellulose, which also had a higher E_H value when compared to RW, signifying a higher degree of hydrogen bonding in the CNC and Cellulose when compared to RW. The order of degree of hydrogen bonding was CNC>Cellulose>RW. This trend is in agreement with previously reported values for E_H for other lignocellulosic materials, where the removal of lignin and amorphous regions in lignocellulosic materials, corresponded to higher degree of hydrogen bonding (Chen *et al.,* 2009; Poletto *et al.,* 2014; Popescu *et al.,* 2007). .

The crystallinity of the RW, cellulose and CNC were also studied by using the indices as proposed by (Nelson and O'Connor, 1964). Lateral order index (LOI), Total Crystallinity Index (TCI) and hydrogen bond index (HBI) values from the FT-IR spectra were determined. The ratio of the bands between 1420-1430 cm^{-1} (which correspond to the number of crystalline regions in the cellulose sample) and the band at 898 cm^{-1} (corresponding to the amorphous region), were used to obtain the LOI value. The LOI corresponds to the relative number of crystalline and amorphous regions in the cellulose.

The TCI value was obtained by taking the ratio of the peaks at 1430 cm^{-1} and 2941 cm^{-1}. The TCI was proposed by Nelson and O'Connor (Nelson and O'Connor, 1964) as an index for the infra-red crystallinity ratio. The degree of crystallinity, chain regularity and amount of bound water were also studied by using the HBI, which is dependent on the bond distance of the cellulose chains and their mobility. The ratio of the bands at 3426 cm^{-1} and 1320 cm^{-1} was assigned to the HBI. The LOI, TCI and HBI values obtained for RW, cellulose and CNC were similar. The LOI values obtained were lower than that reported by Ikhuoria *et al.* (Ikhuoria *et al,* 2015), for CNC from coir. However, the TCI and HBI were similar to the values obtained by Ikhuoria *et al*. The LOI, and HBI values were lower than those reported for *Pinus elliottii, Eucalyptus grandis, Mezilaurus itauba*, and *Dipteryx odorata* (Poletto *et al.,* 2012), while the TCI values for CNC, RW and cellulose from RW, were observed to be slightly higher than those reported by Poletto *et al* (Poletto *et al.,* 2012). The use of LOI, and TCI values in monitoring crystallinity are best suited for comparative studies only, since the assigned spectral regions usually contain contributions from both the amorphous and crystalline chains (Fan *et al.,* 2012).

A considerably higher shift from the free O-H absorption peak (corresponding to a higher degree of hydrogen bonding) should be expected from CNC, considering its higher degree of crystallinity, orientation and close packing of its fibrils than the RW (Moon *et al.,* 2011). The reduced shift observed from the monomeric O-H absorption peak could be because of the effect of the sulphuric acid used during acid hydrolysis of the cellulose. During hydrolysis of the cellulose, some of the O-H groups were esterified, thereby resulting in a reduced degree of hydrogen

bonding (Habibi *et al.,* 2010; Ikhuoria *et al,* 2015; Jiang *et al.,* 2010). The sulphonated hydroxyl groups, apart from reducing the degree of hydrogen bonding, can also help to stabilize the nanocellulose particles by reducing aggregation (Jiang *et al.,* 2010; Ikhuoria *et al,* 2015).

The sulphated hydroxyl group that replaces the hydroxyl group on the cellulose after hydrolysis enhanced the electric double-layer around the CNC particles, thereby increasing the inter-particle repulsion. The effect of this is that, particle-particle aggregation and the degree of hydrogen bonding is reduced. The presence of sulphated groups on the CNC surface, is also expected to promote the steric stabilization characteristics of the synthesized CNC (Mosayabi *et al.,* 2017).

The XRD peaks were assigned to the diffractograms (Figure 2), according to the native cellulose structure, as described by Wada *et al.* (Wada *et al.,* 2001). The diffractograms showed characteristic peaks at 2θ angles of between: 14-14.5°, 16-16.5° and 22-22.5°, corresponding to the ($1\bar{1}0$) (110) and the (200) crystallographic planes, respectively. The 2θ reflection of between 18-18.5°C, which corresponds to the amorphous region of the cellulosic samples was smaller in the CNC diffractogram when compared to

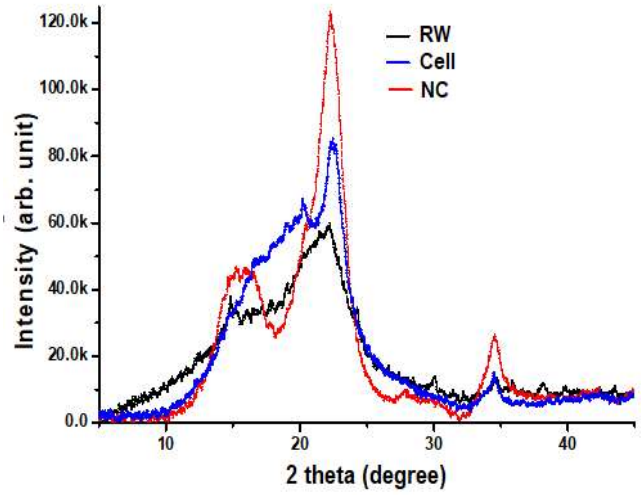

Figure 2: X-ray diffraction patterns of: rubber wood (RW), cellulose (Cell) and nanocellulose (CNC)

the RW and cellulose samples. The reduction in the peak intensity (height) is due to the fact that hydrolysis only occurs at the amorphous regions of cellulose (Moon *et al.,* 2011; Poletto *et al.,* 2014).

The crystallinity index (CI) of the samples was ascertained by using the Segal (Equation 1) and Hermans methods (Poletto *et al.,* 2014; Popescu *et al.,* 2007) (Equation 2). The CI obtained by applying the Segal method shows that the ($1\bar{1}0$) and (110) crystallographic planes are neglected by the Segal method of evaluating *CI*. Hence, values obtained by the Segal method are generally considered inadequate in describing the crystalline state of a lignocellulosic material. It is however, still useful for comparative studies when it is quoted relative to other methods (Ikhuoria *et al,* 2015; Xu iet al., 2013).

The CI and CI' values obtained for RW (65.6%, 63.1%), cellulose (66.4%, 64.3%) and CNC (68.9%, 66.2%) samples, respectively, have progressively increased from RW through to the CNC. This again is, due to the reduction in the proportion of amorphous regions (as predicted by FT-IR) in the lignocellulosic samples, since the treatment of RW *via* the sulphonation route, proceeds to yield CNC. A reduction in the amorphous regions of the nanocrystals, typically increases the crystal orientation and close packing, thereby improving crystallinity (Ikhuoria *et al,* 2015; Moon *et al.,* 2011) of the CNC produced. The crystallinity index values obtained for RW by both the Segal and Herman methods, were higher than those reported for *Pinus elliottii, Eucalyptus grandis, Mezilaurus itauba* and *Dipteryx odorata*, with (*CI*, *CI'*) values of (43.4, 34.1), (49.3, 34.4), (52.7,37.8) and (55.7, 43.0), respectively (Poletto *et al.,* 2014).

Considering the fact that *Pinus elliottii, Eucalyptus grandis, Mezilaurus itauba*, and *Dipteryx odorata*, had similar E_H and R values to RW (16.757, 2.799), (16.182, 2.800), (16.325, 2.800), (16.613, 2.799), respectively, it would have been expected that they exhibit similar *CI* and *CI'* values when compared to RW. However, the lower degrees of crystallinity in *Pinus elliottii, Eucalyptus grandis , Mezilaurus itauba*, and *Dipteryx odorata*, can be attributed to the presence of relatively higher amounts of absorbed water, as reported by Poletto *et al.* (Poletto *et al.,* 2012) and demonstrated by the presence of a band at about $3567cm^{-1}$ in the FT-IR spectra, in all the aforementioned species and the loss of absorbed water at 100°C in their respective thermogravimetric plots (Popescu *et al.,* 2007). The absence of such a band in the FT-IR spectra of RW, shows that absorbed water was minimal (Ikhuoria *et al,* 2015). Absorbed moisture, typically reduces the close packing and molecular orientation of fibers, which consequently reduce crystallinity (Habibi *et al.,* 2010; Azizi Samir *et al.,* 2005; Nainggolan *et al.,* 2013).

Figure 3a shows the morphological assemblies of the CNC in a regular array, as expected for nanocellulose crystals. The measured diameters, obtained for the CNC crystals, were between 10-30 nm with lengths of between 190-300 nm. This is consistent with previously reported studies on CNC crystals particle size (Habibi *et al.,* 2010; Azizi Samir *et al.,* 2005; Nainggolan *et al.,* 2013). As seen from the electron microscope images, slight aggregation of the nanocellulose was observed and this was attributed to the presence of hydrogen bonding in the cellulose nanocrystals (Araki *et al.,* 2000; Araki *et al.,* 1999).

Figure 3b shows the typical distribution of the

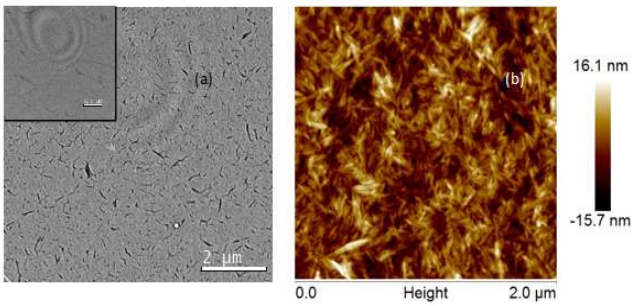

Figure 3: (a) TEM images of CNC and (b) AFM topography images of CNC

population of CNC and the image data height under ambient conditions. The AFM images show regular particle size. This was confirmed by the surface roughness of the CNC, which was found to be c.a. 16 nm. The processed AFM images show that the CNC height (width) was within the range of between 5 to 30 nm and the length was between 130 to 220 nm. The CNC height measurement was consistent across the selected areas measured, although with slight changes within 1 nm run-to-run in the AFM height measurement. These changes in height measurement are often linked with water molecules penetrating the CNC and diffusing between the particles, which generally results to separation in the cellulose chains. This agrees with the report of Lahiji *et al*. (Lahiji *et al.,* 2010), where humidity changes had no effect on the lattice spacing of cellulose, as determined by X-ray diffraction measurements.

The crystal structure and the overall phase purity of the CNC-capped Fe_3O_4 nanoparticles were analysed by using Powder X-ray diffractometer (XRD). The XRD pattern of the magnetic particles (black powder) synthesized is shown in Figure 4(a).

The peaks obtained were indexed in the cubic spinel structure (spatial group Fd-3M group no. 227), JCPDS no: 01-075-0033 for the Fe_3O_4 particles. The XRD pattern indicated that the black powder was Fe_3O_4 (as there was no indication of hematite or partially ordered maghemite) and it was found to be crystalline in nature. This may be attributed to a high pH 12 used, which is consistent with previous report, where Fe^{2+} adsorb at the ferric hydroxide surface (Santoyo *et al.,* 2011), which helped to facilitate the electron hopping between Fe^{2+} and Fe^{3+} (Santoyo *et al.,* 2011; Tronc *et al.,* 1992). The line broadening observed in the diffracted line, indicates the ultrafine nature, crystallite particles and cubic single phase nano-sized Fe_3O_4 powder, which is in accordance with previous reports (Santoyo *et al.,* 2011; Li *et al.,* 2014).

The saturation magnetization (m_s) of CNC-capped magnetite was measured as a function of the magnetic field (H, Oe) at 300 K in the applied magnetic field, ranging between -50 kOe to 50 kOe, as shown in Figure 4(b). At 300 K, the m_s value of 66.7 emu/g for the CNC-capped magnetite synthesized was lower than the M_s of the bulk magnetite (92-100 emu/g) (Han *et al.,* 1994) and this corresponds well with the previously reported works on magnetite nanoparticles of similar sizes and surface functionalization by using chemical co-

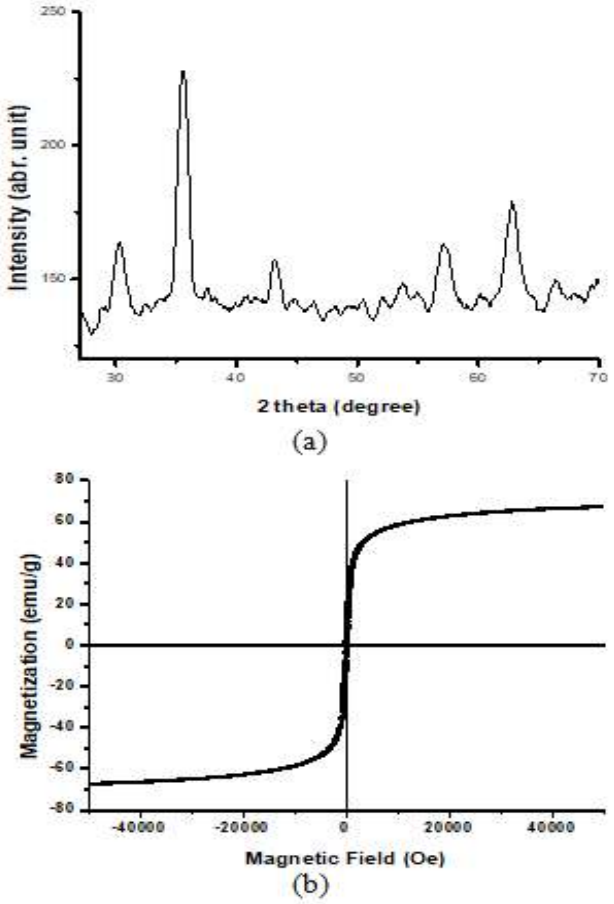

Figure 4: (a) X-Ray diffraction pattern of CNC-capped magnetite showing crystalline peaks of CNC capped Fe_3O_4 nanoparticles by chemical co-precipitation (b) Magnetic hysteresis loop of CNC-capped Fe_3O_4 nanoparticles under magnetic field up to 50 kOe at 300 K

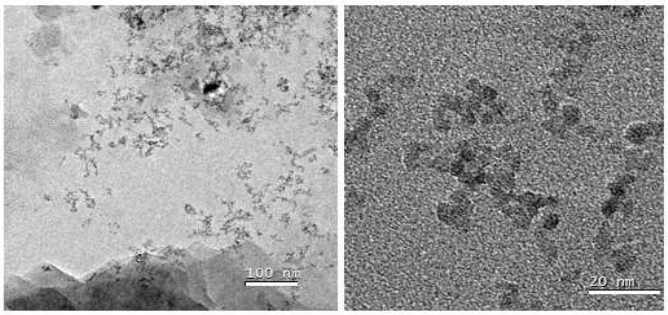

Figure 5: TEM image showing the formation of magnetite nanocrystals capped with nanocellulose at 100 nm (a) and 20 nm (b)

precipitation methods (Tao *et al.,* 2006; Si *et al.,* 2005; Roca *et al.,* 2007).

The low magnetic susceptibility, with respect to particle size in the CNC-capped magnetite, has previously been reported and can be attributed to spin disorder at the particle surface. This is caused by surface in-homogeneities and truncation of the crystalline lattice (Goya *et al.,* 2003; Baumgartner *et al.,* 2013) this is evident in Figure 5. The lower M_s for CNC-capped magnetite may be the combined result of its smaller particle size and the association of Na^+

cations at the particle surface. It was recently shown that the Na^+ cations at the particle surface produced a layer of partially oxidized, non-stoichiometric magnetite/ maghemite that surrounds the crystal core (Panda *et al.,* 2001; Zaitsev *et al.*)

The morphology of the nanocellulose-capped magnetite formed was examined by direct observation *via* transmission electron microscopy (TEM). The TEM images of the magnetite particles (Figure 5) are dominated by particles with very small particle size (~4 nm). The shape of the magnetite nanoparticles was spherical (distorted) or oval in shape, which is typical of magnetite nanoparticles synthesized by chemical co-precipitation (Ghandoor *et al.,* 2012). The Figure further showed that the magnetite nanoparticles were monodispersed with minimal aggregation.

Comparison of the particle size obtained with previous reports for nanomagnetite synthesized by co-precipitation, revealed the effect of the sulphated nanocellulose surface on the size and dispersity of the particles obtained. Specifically, the nanocellulose-capped magnetite nanoparticles obtained, had smaller size and were largely monodispered when compared to previous reports of Jiang *et al*. (Jiang *et al*., 2004), (8-50 nm), Mahdavi *et al*. (Mahdavi *et al*., 2013), (7.83-9.41 nm), Gil *et al*. (Gil *et al*., 2013), 13.80 ± 3.4 nm) and Lee *et al*. (Lee *et al*., 1996), (4-10 nm), who applied different surfactants, for example dextran, oleic acid, dicarboxyl terminated polyethylene glycol and polyvinyl alcohol, respectively.

Reports for nano-magnetite synthesized without surfactant had an average particle size of 16.5 nm and 11.0 nm (obtained *via* control of the pH window applied during synthesis) (Mascolo *et al.,* 2013). The better steric stabilization of nanocellulose when compared to the aforementioned surfactants/ stabilizers, may be attributed to its sulphated hydroxyl groups, larger steric effect and better crystallinity, which reduce inter-particle aggregation and provides the required functional groups for interaction with the nanomagnetite surface. Besides the steric stabilization ability of the above surfactants/stabilizers, other factors, such as: the pH of the solution, stirring rate, duration of heat treatment, etc., may have also contributed to the results obtained (Mahdavi *et al.,* 2013).

The small size of the nanocellulose stabilized nanomagnetite particles implies that they are single domain particles. Since shape anisotropy is known to be absent in spherically-shaped single domain particles, the nanocellulose-capped nanomagnetite particles synthesized, exhibited superparamagnetic behaviour (as seen in **Figure 4b**) (Laurent *et al.,* 2008).

4. CONCLUSION

The challenges in the synthesis of magnetite nanoparticles *via* the chemical co-precipitation route are the polydispersity and large particle sizes that are sometimes obtained. However, chemical co-precipitation is a highly desirable approach for the synthesis of magnetite nanoparticles, especially for bio-medical applications, due to the ease of the method and the ready availability of its reagents. Typically, surfactants or steric stabilizers are applied to control the particle growth and aggregation and hence, produce monodispersed nanoparticles with acceptable size range. The choice of surfactant or steric stabilizer depends on their ability to stabilize the nanoparticles against Van der Waals attractive forces, which promote aggregation during the nucleation and growth processes. This is achieved *via* the electric double layer repulsion or steric stabilization or a combination of both.

In this work, nanocellulose crystals were synthesized from RW and its pendant hydroxyl groups functionalized *in-situ via* sulphuric acid hydrolysis in order to obtain sulphated nanocrystals. The sulphating of the nanocrystals reduced the hydrogen bonding in the nanocellulose and hence, resulting in less aggregation in CNC, while improving its ability to stabilize nanomagnetite particles by increasing the length of the electric double-layer and steric stabilization. The nanocellulose-capped magnetite particles obtained, were monodispered and are of relatively small size when compared to previous reports that employed other surfactants, such as: dextran, oleic acid, dicarboxyl terminated polyethylene glycol and polyvinyl alcohol. The nanomagnetite particles obtained were spherical, of single domain particle size range and they exhibited good colloidal stability as ferrofluid.

REFERENCES

Abraham, E., Deepa, B., Pothen, L.A., Cintil, J., Thomas, S., John, M.J., Anandjiwala, R. and Narine, S.S. (2013). "Environmental friendly method for the extraction of coir fibre and isolation of nanofibre." Carbohydrate Polymers, 92(2):1477-1483.

Araki, J., Wada, M., Kuga, S. and Okano, T. (1999). "Influence of surface charge on viscosity behavior of cellulose microcrystal suspension." Journal of Wood Science, 45(3):258-261.

Araki, J., Wada, M., Kuga, S. and Okano, T. (2000). "Birefringent Glassy Phase of a Cellulose Microcrystal Suspension." Langmuir, 16(6): 2413-2415.

Azizi Samir, M.A.S., Alloin, F. and Dufresne, A. (2005). "Review of Recent Research into Cellulosic Whiskers, Their Properties and Their Application in Nanocomposite Field." Biomacromolecules, 6(2): 612-626.

Baumgartner, J., Dey, A., Bomans, P.H.H., Le Coadou, C., Fratzl, P., Sommerdijk, N.A.J.M. and Faivre, D. (2013). "Nucleation and growth of magnetite from solution." Nat Mater, 12(4): 310-314.

Cao, X., Dong, H. and Li, C.M. (2007). "New Nanocomposite Materials Reinforced with Flax Cellulose Nanocrystals in Waterborne Polyurethane." Biomacro-molecules, 8(3): 899-904.

Chen, Y., Liu, C., Chang, P.R., Cao, X. and Anderson, D. P. (2009). "Bionanocomposites based on pea starch and cellulose nanowhiskers hydrolyzed from pea hull fibre: Effect of hydrolysis time." Carbohydrate Polymers, 76(4): 607-615.

Choi, Y. and Simonsen, J. (2006). "Cellulose nanocrystal-filled carboxymethyl cellulose nanocomposites." J Nanosci Nanotechnol, 6(3): 633-639.

Durdureanu-Angheluta, A., Pinteala, M. and Simionescu, B.C. (2012). "Tailored and functionalized magnetite nanoparticles for biomedical and industrial applications."Materials Science and Technology, Prof. Sabar Hutagalung (Ed.), ISBN: 978-953-51-0193-2

Fan, M., Dai, D. and Huang, B. (2012). "Fourier Transform Infrared Spectroscopy for Natural Fibres." In: Fourier Transform - Materials Analysis, Salih, D.S. (ed.), ISBN: 978-953-51-0594-7.

Favier, V., Chanzy, H. and Cavaille, J.Y. (1995). "Polymer Nanocomposites Reinforced by Cellulose Whiskers." Macromolecules, 28(18): 6365-6367.

Garcia de Rodriguez, N.L., Thielemans, W. and Dufresne, A. (2006). "Sisal cellulose whiskers reinforced polyvinyl acetate nanocomposites." Cellulose, 13(3): 261-270.

Ghandoor, H. E., Zidan, H. M., Mostafa, M.H.K. and mail, M.I. (2012). "Synthesis and Some Physical Properties of Magnetite (Fe_3O_4) Nanoparticles. International Journal of Electrochemical Science, 7: 5734 - 5745.

Gil, S., Castro, E. and Mano, J.F. (2013). "Synthesis and characterization of stable dicarboxylic pegylated magnetite nanoparticles." Materials Letters, 100:266-270.

Goya, G.F., Berquó, T. S., Fonseca, F.C. and Morales, M.P. (2003). "Static and dynamic magnetic properties of spherical magnetite nanoparticles." Journal of Applied Physics, 94(5): 3520-3528.

Grunert, M. and Winter, W.T. (2002). "Nanocomposites of Cellulose Acetate Butyrate Reinforced with Cellulose Nanocrystals." Journal of Polymers and the Environment, 10(1):27-30.

Habibi, Y., Goffin, A.-L., Schiltz, N., Duquesne, E., Dubois, P. and Dufresne, A. (2008). "Bionanocomposites based on poly(ε-caprolactone)-grafted cellulose nanocrystals by ring-opening polymerization." Journal of Materials Chemistry, 18(41): 5002-5010.

Habibi, Y., Lucia, L.A. and Rojas, O.J. (2010). "Cellulose Nanocrystals: Chemistry, Self-Assembly, and Applications." Chemical Reviews, 110(6): 3479-3500.

Han, D.H., Wang, J.P. and Luo, H.L. (1994). "Crystallite size effect on saturation magnetization of fine ferrimagnetic particles." Journal of Magnetism and Magnetic Materials, 136(1): 176-182.

Hubbe, M.A., Rojas, O.J., Lucia, L.A. and Sain, M. (2008). "Cellulosic Nanocomposites: A Review." BioResources, 3(3): 929-980

Ikhuoria, E.U., Omorogbe, S.O., Agbonlahor O.G. and Etiuma, R.A. (2015). "Nanocellulose Crystals from Coir Fibre for Template Application." American Chemical Science Journal, 9(1): 1-11.

Jiang, F., Esker, A.R. and Roman, M. (2010). "Acid-Catalyzed and Solvolytic Desulfation of H_2SO_4 -Hydrolyzed Cellulose Nanocrystals." Langmuir, 26(23): 17919-17925.

Jiang, W., Yang, H.C., Yang, S.Y., Horng, H.E., Hung, J.C., Chen, Y.C. and Hong, C.Y. (2004). "Preparation and properties of superparamagnetic nanoparticles with narrow size distribution and biocompatible." Journal of Magnetism and Magnetic Materials, 283(2): 210-214.

Lahiji, R.R., Xu, X., Reifenberger, R., Raman, A., Rudie, A. and Moon, R.J. (2010). "Atomic Force Microscopy Characterization of Cellulose Nanocrystals." Langmuir, 26(6): 4480-4488.

Laurent, S., Forge, D., Port, M., Roch, A., Robic, C., Vander Elst, L. and Muller, R. N. (2008). "Magnetic Iron Oxide Nanoparticles: Synthesis, Stabilization, Vectorization, Physicochemical Characterizations, and Biological Applications." Chemical Reviews, 108(6): 2064-2110.

Lee, J., Isobe, T. and Senna, M. (1996). "Magnetic properties of ultrafine magnetite particles and their slurries prepared via in-situ precipitation." Colloids and Surfaces A: Physicochemical and Engineering Aspects, 109:121-127.

Li, X., Liu, D., Song, S. and Zhang, H. (2014). "Fe_3O_4@SiO_2@TiO_2@Pt Hierarchical Core–Shell Microspheres: Controlled Synthesis, Enhanced Degradation System, and Rapid Magnetic Separation to Recycle." Crystal Growth and Design, 14(11): 5506-5511.

Lin, C.L., Lee, C.-F. and Chiu, W.Y. (2005). "Preparation and properties of poly(acrylic acid) oligomer stabilized superparamagnetic ferrofluid. Journal of Colloid and Interface Science, 291(2): 411-420.

Mahdavi, M., Ahmad, M., Haron, M., Namvar, F., Nadi, B., Rahman, M. and Amin, J. (2013). "Synthesis, Surface Modification and Characterisation of Biocompatible Magnetic Iron Oxide Nanoparticles for Biomedical Applications." Molecules, 18(7): 7533.

Mahmoudi, M., Simchi, A., Imani, M., Milani, A. S. and Stroeve, P. (2008). "Optimal Design and Characterization of Superparamagnetic Iron Oxide Nanoparticles Coated with Polyvinyl Alcohol for Targeted Delivery and Imaging." The Journal of Physical Chemistry B, 112(46): 14470-14481.

Mascolo, M., Pei, Y. and Ring, T. (2013). "Room Temperature Co-Precipitation Synthesis of Magnetite Nanoparticles in a Large pH Window with Different Bases." Materials, 6(12): 5549.

Massart, R. (1981). "Preparation of aqueous magnetic liquids in alkaline and acidic media." IEEE Trans Magn., 17:1247-1248.

Massart, R., Dubois, E., Cabuil, V. and Hasmonay, E. (1995). "Preparation and properties of monodisperse magnetic fluids." Journal of Magnetism and Magnetic Materials, 149(1–2):1-5.

Mondini, S., Cenedese, S., Marinoni, G., Molteni, G., Santo, N., Bianchi, C.L. and Ponti, A. (2008). "One-step synthesis and functionalization of hydroxyl-decorated magnetite nanoparticles." Journal of colloid and interface science, 322(1):173-179.

Moon, R.J., Martini, A., Nairn, J., Simonsen, J. and Youngblood, J. (2011). "Cellulose nanomaterials review: structure, properties and nanocomposites." Chemical Society Reviews, 40(7):3941-3994.

Mosayebi, J., Kiyasatfar, M. and Laurent, S. (2017). "Synthesis, Functionalization, and Design of Magnetic Nanoparticles for Theranostic Applications." Advanced Healthcare Materials, 6(23):1700306.

Nainggolan, H., Gea, S., Bilotti, E., Peijs, T. and Hutagalung, S.D. (2013). "Mechanical and thermal properties of bacterial-cellulose-fibre-reinforced Mater-Bi(®) bionanocomposite." Beilstein Journal of nanotechnology, 4:325-329.

Nelson, M. L. and O'Connor, R. T. (1964). "Relation of certain infrared bands to cellulose crystallinity and crystal latticed type." Part I. Spectra of lattice types I, II, III and of amorphous cellulose. Journal of Applied Polymer Science, 8(3): 1311-1324.

Oksman, K. and Sain, M. (2006). "Cellulose Nanocomposites." (ed) American Chemical Society ISBN13: 9780841239807; eISBN: 9780841220560

Panda, RN., Gajbhiye, N.S. and Balaji, G. (2001). "Magnetic properties of interacting single domain Fe_3O_4 particles. Journal of Alloys and Compounds, 326(1): 50-53.

Paralikar, S.A., Simonsen, J. and Lombardi, J. (2008). "Poly(vinyl alcohol)/cellulose nanocrystal barrier membranes." Journal of Membrane Science, 320(1): 248-258.

Poletto, M., Ornaghi, H.L. and Zattera, A.J. (2014). "Native Cellulose: Structure, Characterization and Thermal Properties." Materials, 7(9): 6105-6119.

Poletto, M., Zattera, A.J., Forte, M. M.C. and Santana, R.M.C. (2012). "Thermal decomposition of wood: influence of wood components and cellulose crystallite size." Bioresource technology, 109:148-153.

Popescu, C.M., Popescu, M. C., Singurel, G., Vasile, C., Argyropoulos, D.S. and Willfor, S. (2007). "Spectral Characterization of Eucalyptus Wood." Applied Spectroscopy, 61(11): 1168-1177.

Ravikumar, C. and Bandyopadhyaya, R. (2011). "Mechanistic Study on Magnetite Nanoparticle Formation by Thermal Decomposition and Coprecipitation Routes.: The Journal of Physical Chemistry C, 115(5): 1380-1387.

Roca, A.G., Marco, J.F., Morales, M.D,P. and Serna, C.J. (2007). "Effect of Nature and Particle Size on Properties of Uniform Magnetite and Maghemite Nanoparticles." The Journal of Physical Chemistry C, 111(50): 18577-18584.

Rosa, M.F., Medeiros, E.S., Malmonge, J.A., Gregorski, K.S., Wood, D.F., Mattoso, L. H. C., Glenn, G., Orts, W. J. and Imam, S.H. (2010). "Cellulose nanowhiskers from coconut husk fibers: Effect of preparation conditions on their thermal and morphological behavior." Carbohydrate Polymers, 81(1): 83-92.

Santoyo Salazar, J., Perez, L., de Abril, O., Truong Phuoc, L., Ihiawakrim, D., Vazquez, M., Greneche, J.-M., Begin-Colin, S. and Pourroy, G. (2011). "Magnetic Iron Oxide Nanoparticles in 10−40 nm Range: Composition in Terms of Magnetite/Maghemite Ratio and Effect on the Magnetic Properties." Chemistry of Materials, 23(6): 1379-1386.

Sèbe, G., Ham-Pichavant, F., Ibarboure, E., Koffi, A. L. C. and Tingaut, P. (2012). "Supramolecular Structure Characterization of Cellulose II Nanowhiskers Produced by Acid Hydrolysis of Cellulose I Substrates." Biomacromolecules, 13(2): 570-578.

Shukla, A., Degen, P. and Rehage, H. (2007). "Synthesis and Characterization of Monodisperse Poly(organosiloxane) Nanocapsules with or without Magnetic Cores." Journal of the American Chemical Society, 129(26): 8056-8057.

Si, S., Li, C., Wang, X., Yu, D., Peng, Q. and Li, Y. (2005). "Magnetic Monodisperse Fe3O4 Nanoparticles." Crystal Growth and Design, 5(2): 391-393.

Tao, K., Dou, H. and Sun, K. (2006). "Facile Interfacial Coprecipitation To Fabricate Hydrophilic Amine-Capped Magnetite Nanoparticles." Chemistry of Materials, 18(22): 5273-5278.

Tronc, E., Belleville, P., Jolivet, J. P. and Livage, J. (1992). "Transformation of ferric hydroxide into spinel by iron(II) adsorption." Langmuir, 8(1): 313-319.

Wada, M., Okano, T. and Sugiyama, J. (2001). "Allomorphs of native crystalline cellulose I evaluated by two equatoriald-spacings." Journal of Wood Science, 47(2): 124-128.

Wang, T., Cai, Z., Liu, L., Bayer, I. S. and Biswas, A. 2010. Nanotechnology : emerging applications of cellulose-based green magnetic nanocomposites. Vacuum technology and coating., 11(9): 2-5.

Xu, F., Shi, Y.-C. and Wang, D. (2013). "X-ray scattering studies of lignocellulosic biomass: a review." Carbohydrate polymers, 94(2): 904-917.

Zaitsev, V. S., Filimonov, D. S., Presnyakov, I. A., Gambino, R. J. and Chu, B. (1999). "Physical and Chemical Properties of Magnetite and Magnetite-Polymer Nanoparticles and Their Colloidal Dispersions." Journal of Colloid and Interface Science, 212(1): 49-57.

Zhan, H. Y., Zhou, Y. M., Zheng, L. M. and Fu, S. Y. (2012). "Effect of nanocellulose isolation techniques on the formation of reinforced poly(vinyl alcohol) nanocomposite films." eXPRESS Polymer Letters,